Calcium sensitive ring-like oligomers formed by synaptotagmin

Jing Wang (晶)[a], Oscar Bello[a], Sarah M. Auclair[a], Jing Wang (璟)[b], Jeff Coleman[a], Frederic Pincet[a,c], Shyam S. Krishnakumar[a], Charles V. Sindelar[d,1], and James E. Rothman[a,b,1]

Departments of [a]Cell Biology, [b]Chemistry, and [d]Molecular Biophysics and Biochemistry, Yale University School of Medicine, New Haven, CT 06520; and [c]Laboratoire de Physique Statistique, Unité Mixte de Recherche, Centre National de la Recherche Scientifique, 8550 Associée aux Universités Paris 6 et Paris 7, Ecole Normale Supérieure, 75005 Paris, France

Contributed by James E. Rothman, August 15, 2014 (sent for review May 27, 2014; reviewed by Thomas Söllner and Nikolaus Grigorieff)

The synaptic vesicle protein synaptotagmin-1 (SYT) is required to couple calcium influx to the membrane fusion machinery. However, the structural mechanism underlying this process is unclear. Here we report an unexpected circular arrangement (ring) of SYT's cytosolic domain (C2AB) formed on lipid monolayers in the absence of free calcium ions as revealed by electron microscopy. Rings vary in diameter from 18–43 nm, corresponding to 11–26 molecules of SYT. Continuous stacking of the SYT rings occasionally converts both lipid monolayers and bilayers into protein-coated tubes. Helical reconstruction of the SYT tubes shows that one of the C2 domains (most likely C2B, based on its biochemical properties) interacts with the membrane and is involved in ring formation, and the other C2 domain points radially outward. SYT rings are disrupted rapidly by physiological concentrations of free calcium but not by magnesium. Assuming that calcium-free SYT rings are physiologically relevant, these results suggest a simple and novel mechanism by which SYT regulates neurotransmitter release: The ring acts as a spacer to prevent the completion of the soluble *N*-ethylmaleimide–sensitive factor activating protein receptor (SNARE) complex assembly, thereby clamping fusion in the absence of calcium. When the ring disassembles in the presence of calcium, fusion proceeds unimpeded.

Synaptotagmin-1 (SYT) is the calcium (Ca^{2+}) sensor that triggers synchronous release of neurotransmitters for synaptic transmission (1–4). It is a transmembrane protein, localized to the synaptic vesicles (1, 5), with tandem cytosolic C2 domains (C2A and C2B) that bind phospholipids in both a Ca^{2+}-independent and a Ca^{2+}-dependent manner (1, 6). The membrane-distal C2B domain interacts with acidic lipids such as phosphatidylserine (PS) and phosphatidylinositol 4,5-bisphosphate (PIP_2) to mediate efficient docking of the synaptic vesicles (7–10) before the influx of Ca^{2+} ions. Recent studies (7, 8, 11, 12) have located this calcium-independent membrane-binding site to a polybasic patch on the C2B domain (site I in Fig. 1*A*). The binding of Ca^{2+} to the calcium-coordination pocket of the C2B domain (site II in Fig. 1*A*) triggers the insertion of flanking portions of site II into the plasma membrane, and this Ca^{2+}-triggered membrane insertion is absolutely required for neurotransmitter release (13–16).

The C2B domain also mediates the Ca^{2+}-independent binding of SYT to neuronal soluble *N*-ethylmaleimide–sensitive factor activating protein receptor on the plasma membrane (t-SNARE) [syntaxin/ synaptosomal-associated protein 25 (SNAP25)], most likely via its interaction with SNAP25 (17-21). This interaction is believed to position SYT on the prefusion SNARE complexes to trigger rapid exocytosis in response to Ca^{2+} (20, 22). How the insertion of site II into the membrane bilayer is coupled to the completion of the SNARE assembly to release neurotransmitter is still unclear, although some key points have been established. In the prefusion state, the SNARE complexes are clamped at a half-zippered state and are prevented from further assembly by a mechanism involving SYT and the synaptic protein complexin (CPX) (23–27). Upon calcium binding, the C2 domain and t-SNAREs retain a fixed spatial relationship as site II rapidly inserts into the bilayer (20), suggesting that if cooperative conformational changes are involved in calcium coupling, they likely involve a higher-order oligomeric arrangement of these proteins.

To understand how Ca^{2+} binding to SYT triggers the completion of the SNARE complex assembly to drive fusion, we are exploring the supramolecular organization that SYT can assume on membrane surfaces. Here, we have used EM to visualize the organization of membrane-bound SYT-C2AB domains in the absence of calcium. We report that SYT-C2AB domains assemble into ring-like structures on lipid monolayers under Ca^{2+}-free conditions. This oligomeric assembly requires the electrostatic interaction of SYT with PS in the lipid monolayers. These rings enclose and deform the lipid surface and disassemble upon exposure to physiological levels of Ca^{2+} ions, suggesting a novel mechanism by which SYT regulates neurotransmitter release.

Results

SYT-C2AB Domains Oligomerize as Circular Structures on the Membrane Surface. To obtain oligomeric SYT-C2AB domains on lipid surfaces, we adapted the conditions used for 2D crystallization of protein kinase C (28), combined with the affinity grid technique (29). Briefly, the lipid monolayer formed at the air/water interface was recovered by placing a carbon-coated EM grid on top of the lipid hydrophobic tails. After the lipid was transferred onto an EM grid, protein solution was added to the lipid monolayer under Ca^{2+}-free conditions (1 mM EDTA) and was incubated for 1 min at room temperature (22 °C). Negative-staining EM analysis revealed the presence of ring-like structures on the lipid monolayer

Significance

Synaptotagmin-1 is the calcium sensor for synchronous neurotransmitter release. It couples calcium influx to the soluble *N*-ethylmaleimide–sensitive factor activating protein receptor (SNARE)-catalyzed fusion, but how this coupling happens is unknown. Here, using electron microscopy, we report that the cytosolic domain of synaptotagmin can assemble into ring-like oligomers under calcium-free conditions, and these rings disassemble rapidly upon calcium binding. This process suggests a novel but speculative mechanism to explain calcium coupling, in which the synaptotagmin rings separate the vesicle and plasma membranes and prevent the completion of SNARE complex assembly until the influx of calcium.

Author contributions: Jing Wang, F.P., S.S.K., C.V.S., and J.E.R. designed research; Jing Wang, O.B., S.M.A., and Jing Wang performed research; J.C. contributed new reagents/analytic tools; Jing Wang, O.B., S.M.A., F.P., S.S.K., C.V.S., and J.E.R. analyzed data; and Jing Wang, S.S.K., C.V.S., and J.E.R. wrote the paper.

Reviewers: T.S., University of Heidelberg; and N.G., Howard Hughes Medical Institute, Janelia Farm Research Campus.

The authors declare no conflict of interest.

[1]To whom correspondence may be addressed. Email: charles.sindelar@yale.edu or james.rothman@yale.edu.

This article contains supporting information online at www.pnas.org/lookup/suppl/doi:10.1073/pnas.1415849111/-/DCSupplemental.

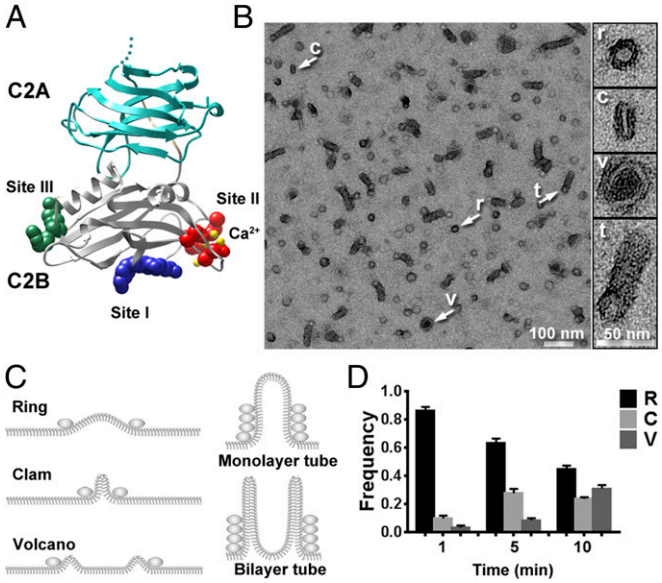

Fig. 1. Calcium-free SYT-C2ABs form circular oligomers on a lipid monolayer surface. (*A*) Atomic structure of the SYT-C2AB domain (PDB ID code 2R83). The C2A domain (residues 96–263) and C2B domain (residues 271–421) are shown in cyan and gray, respectively. The calcium-independent lipid-binding site (site I) consists of four lysine residues (K324, K325, K326, and K327; blue) (12, 39). The calcium-dependent lipid-binding site (site II) consisting of four conserved aspartic residues (D303, D309, D363, and D365; red) coordinates the binding of calcium ions (yellow), which are superimposed from a calcium-bound structure of C2AB [PDB I code 2YOA (53)]. In the arginine apex (site III), conserved arginine residues (R398 and R399; green) might be involved in membrane aggregation (10). (*B*) (*Left*) Ring-like SYT-C2AB oligomers appeared after 1-min incubation on lipid monolayer in the absence of Ca^{2+} at room temperature, as visualized by negative-staining EM. (*Right*) Enlarged view of the oligomeric structures: ring (r), clam (c), volcano (v), and tubule (t). (*C*) Schematics of possible pathways by which the lipid monolayer can be remodeled by SYT oligomers (cross-section). The circular SYT oligomer (ring) could buckle the lipid monolayer into a dome. Because of the instability of lipid monolayer, the dome might seal laterally into a bilayer bar sandwiched by SYT molecules (clam), or the buckled monolayer might collapse vertically so that the center of the monolayer reattaches to the carbon film below and the edge folds into a bilayer rim surrounded by SYT (volcano). Also, the continuous stacking of the SYT oligomer might elongate the lipid into either a monolayer tube from a ring or into bilayer tube from a volcano. (*D*) Quantification of oligomeric SYT-C2AB structures shows the evolution of ring-like structures. Syt-C2AB (5 uM) was incubated with lipid monolayer for various times (1, 5, or 10 min) at 37 °C. C, clam; R, ring; V, volcano. The number of each type of structure was normalized to the total number of oligomeric structures counted on each micrograph to cancel any dispersion of distribution.

(Fig. 1*B*). In lightly stained areas of the grid, SYT rings appeared dark, probably because the stain collected around the protein. In a darkly stained area of a grid many of these rings showed bright bands around the periphery, representing zones of true negative staining (Fig. 2*C*).

Besides the circular rings, we also observed related oligomers including "clams," "volcanos," and "tubes" (Fig. 1*B*). Clams consist of a bright linear feature sandwiched between two layers of proteins. We interpret these features as rings that have collapsed laterally, buckling the central monolayer region to form a bilayer sandwiched between two SYT layers (Fig. 1*C*). Volcanos consist of expanded ring-like structures with a shallow center and a bilayer edge further surrounded by a layer of protein (Fig. 1*B*). Volcanos might correspond to collapsed ring structures (Fig. 1*C*). The percentage of these alternate structures increased with a proportional decrease in the percentage of SYT rings as incubation times were lengthened (Fig. 1*D*), indicating that the rings are kinetic precursors to the clams and volcanos. Therefore, we concluded the ring is the most relevant arrangement of the SYT protein. In support of this assumption, we also observed tubular protein-coated structures growing out of lipid monolayers and bilayers (Fig. 1*B*; also see Fig. S4) that appear to be closely related to the ring structures (see below).

The diameter of these SYT rings ranged from 18–43 nm, with an average size of 27.6 ± 0.6 nm (mean ± SD) (Fig. 2*A*) corresponding to 11–26 copies of SYT per ring (interpolated from the helical symmetry of SYT-decorated tubes, as discussed below). Despite the variation in outer diameter (Fig. 2*B*), each ring is composed of a band of constant width surrounding a circular stain-excluded region. The width of the band, about 50 Å, is consistent with the dimensions of a single SYT-C2AB domain (30). Unexpectedly, the stain-excluded regions within the rings appeared brighter than the background under true-negative staining conditions (Fig. 2*C*). Given the lipid-bending property of SYT (11, 31), a probable explanation for the exclusion of stain from the centers of the rings is that the lipid monolayer in these regions has been displaced upwards (buckled) by the surrounding SYT proteins (Fig. 1*C*).

Ring Assembly Is Specific to the SYT-C2AB Domain. Ring-like structures are a unique and intrinsic property of the calcium-free SYT-C2AB domain. A lipid monolayer treated with buffer or incubated with other proteins (BSA, SNARE/complexin complex) did not show ring-like structures but rather appeared as a heterogeneous pattern (Fig. S1). Furthermore, increasing the input SYT concentration caused a corresponding increase in the number of rings observed on the lipid monolayers (Fig. S2), indicating that ring formation requires the presence of SYT. These findings indicated that these rings are not artifacts of the negative staining procedure, a conclusion that is supported further by the presence of ring-like structures of similar dimension observed by cryo-EM (Fig. S3).

The number and integrity of SYT rings were affected significantly by anionic lipids present in the monolayer and the ionic strength of the buffer used. A minimum of 35% PS was required to obtain stable ring structures (Fig. S2). Ring formation did not require PIP_2, because similar numbers of rings were observed on phosphatidylcholine (PC)/PS monolayers (40% PS: 9.9 ± 0.9 rings per um^2; 25% PS: 0.5 ± 0.5 rings per um^2, mean ± SEM) and on PC/PS monolayers supplemented with 5% PIP_2 (40% PS + 5% PIP_2: 11.5 ± 1.5 rings per um^2; 25% PS + 5% PIP_2: 1.2 ± 0.2 rings per um^2). Therefore, we excluded PIP_2 from our lipid monolayer assay to simplify the membrane composition and typically used a monolayer composed of 1-palmitoyl-2-oleoyl-sn-glycero-3-phosphocholine (POPC) and 1,2-dioleoyl-sn-glycero-3-phospho-L-serine (DOPS) at a 3:2 molar ratio. The assembly of the SYT ring also was sensitive to the ionic strength of the buffer. The ideal salt concentration was 15 mM KCl, and buffers containing 50 mM KCl inhibited ~75% of ring formation (Fig. S2). In addition, mutation of the key lysine residues (K326A, K327A) within the polybasic patch on C2B domain (site I in Fig. 1*A*) drastically reduced the number of SYT rings, by ~95% (Fig. S2). Taken together, these results suggested that the electrostatic interaction between the polybasic patch of C2B (site I) and the negatively charged phospholipids is critical for the formation of SYT rings. Note: The SYT construct tested here contains only the cytoplasmic C2AB domain of SYT (residues 143–421). In the full-length protein, the 60-residue linker region that connects the C2 domain to the membrane anchor, which is known to self-oligomerize (1, 32, 33), might help stabilize the circular ring-like arrangement under physiological salt concentrations.

We optimized the conditions that form rings (Fig. 2*C*) and performed 2D class averaging of the resulting rings. This analysis revealed two shells of densities surrounding a central stain-excluded area (Fig. 2*D*). However, neither symmetry reinforcement

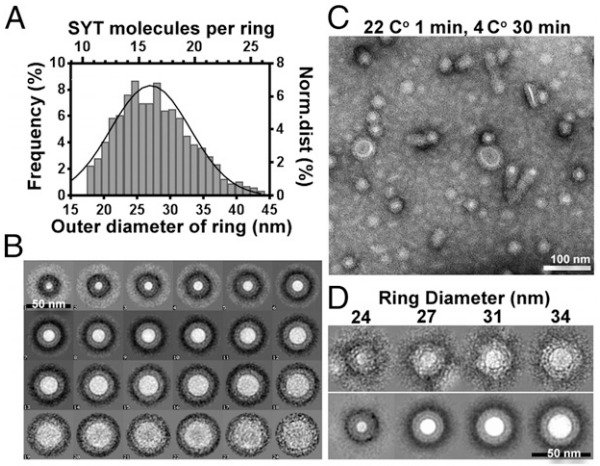

Fig. 2. Structural analysis of SYT rings. (*A*) The size distribution of SYT rings was measured from the outer diameter (n = 985). Ring particles were aligned to a series of discs of increasing size by multireference alignment. The number of particles sorted into each class was normalized to the total number of input particles to represent the frequency of SYT rings at each diameter bin (lower x axis). We determined there were 22 SYT molecules in a bilayer tube with a diameter of 37 nm, giving a SYT/diameter ratio of 0.6. Using this value, we calculated the number of SYT molecules per ring for a given diameter (upper x axis). (*B*) Average of ring particles corresponding to each diameter bin as shown in *A*. (*C*) Optimized SYT rings visualized by negative staining. The protein solution was incubated on an EM grid-supported monolayer at 22 °C for 1 min, followed by annealing on ice for 30 min. (*D*) Circular arrangement of SYT. (*Upper*) Representative SYT-C2AB rings varying by diameter. (*Lower*) The corresponding class averages determined by multivariate statistical analysis. The center of the ring appears white, probably because the monolayer is buckled and raised above the level of the stain, given the lipid-bending property of SYT (11, 31). The density surrounding the central lipid domain shows a two-shell feature that might correspond to the tandem C2A-C2B domain of SYT.

nor class-averaging analysis could resolve features corresponding to individual SYT subunits, leaving the protein architecture underlying the ring structure unclear. We suspected that the tube structures in our sample represented spiral extensions of the rings that protruded from the membrane, and some of the rings may represent the end-on views of short tubules. Therefore we performed helical reconstruction of the SYT-C2AB–decorated tubes to determine the structure of the SYT rings.

SYT-C2AB Domain Induces the Formation of Membrane Tubes. The SYT-coated tubes observed in the lipid monolayer system had multiple sources of origin (Fig. S4). There were lipid monolayer tubules budding directly from underlying lipid monolayer, lipid bilayer tubes emanating from the volcano structures (34), and lipid bilayer tubes that extended from liposomes attached to the lipid monolayer (Fig. S4). Tube formation seemed to be driven by the spiral extension of SYT rings, which facilitate the extension of membrane tubes. These tubes are different from the previously characterized tubular structures (11) induced by SYT. First, these tubes were formed under Ca^{2+}-free conditions, compared with the strict requirement of Ca^{2+} in the earlier reports (11, 31). Second, these tubes were significantly wider, with a mean diameter of 29.1 ± 3 nm for the monolayer-derived tubes and 37.5 ± 6 nm for the bilayer-derived tubes (Fig. S4), compared with the 17.5 ± 3 nm mean diameter for calcium-induced tubules from Folch liposomes (11). Last, the most significant difference was that calcium-free tubes were coated with proteins (Fig. 3*A* and Fig. S5), whereas the membrane-only tubules formed in the presence of calcium. In fact, some of these ordered tubes had a distinctive diffraction pattern allowing their 3D structure to be determined by helical reconstruction (Fig. 3*B* and Fig. S5).

Because only a minority of the monolayer tubes gave a distinct diffraction pattern suitable for helical indexing (Fig. S5), we focused on the bilayer tubes for a detailed analysis. The diameter of bilayer-derived SYT-C2AB tubes varied from 20–50 nm (Fig. S4), corresponding to different helical families. As defined by the start numbers of two principal helices of a helical lattice (35), the most frequently encountered tubes belong to the (−4, 19), (−4, 21), (−4, 22), and (−4, 25) families. These families had mean diameters of 32.7 ± 0.1, 35.2 ± 0.4, 37.5 ± 0.5, and 41.7± 0.04 nm, respectively, with some intrafamily variations caused by flattening and slight differences in unit cell dimensions. This linear correlation between the diameter of SYT tube and its helical start number was used to interpolate the number of SYT molecules in a single ring with a given diameter (Fig. 2*A*).

We reconstructed the helical family (−4, 22) using a single-particle method, iterative helical real space reconstruction (IHRSR) (36, 37). Diffraction patterns from individual tubes did not show layer lines extending beyond 39 Å (Fig. 3*B*). However, by aligning and averaging images of tubes from the same helical family (Fig. S6), we were able to reconstruct a 3D structure of the SYT-C2AB tubular array (Fig. 3*C*) at 24.2-Å resolution assessed by gold-standard Fourier shell correlation ($FSC_{0.143}$) (Fig. S6). As shown in the cross-sections of reconstructed tubes (Fig. 3 and Fig. S7), the shape of asymmetric unit of the helical array resembled an elongated structure normal to the helix axis. The dimensions of asymmetric unit, about 50 Å long from the lipid/protein interface to the outer boundary of the protein and with a thickness of 40 Å, are consistent with the dimensions of a single calcium-free SYT-C2AB molecule (30). In addition, the cross-section of the reconstructed SYT tube matched the ring-class average of the same diameter (Fig. 3*A*, *Lower*), suggesting a similar arrangement of SYT molecules in rings and tubes. Therefore we concluded that the rings represented end-on views of one or more turns of the SYT helices. This structural feature may greatly increase the heterogeneity of selected "rings," even those with a

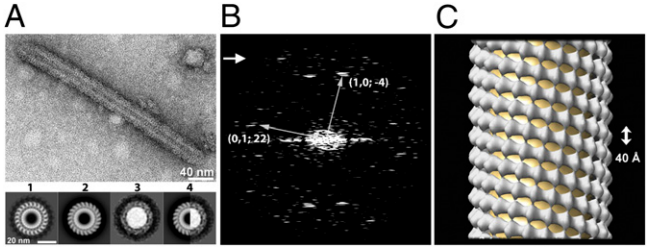

Fig. 3. Structural analysis of a SYT-C2AB–decorated tube. (*A*) Electron micrograph of a SYT-C2AB–decorated tube visualized by negative staining. The protein arrangement in the SYT-decorated tube is comparable to that in a SYT ring because the cross-section of the 3D-reconstructed SYT tube matches the SYT ring class average at the same diameter. (*1*) A cross-section normal to the tube axis from the 3D helical reconstruction of a single tube. The membrane tube is surrounded by 22 subunits of C2AB. The thickness of the membrane is about 5 nm, corresponding to a phospholipid bilayer. (*2*) Cross-section of the averaged reconstruction of the (−4, 22) helical family (n = 5). (*3*) Class average of rings with a 37-nm diameter (n = 21). (*4*) The right half of the tube cross-section in *2* matches the left half of the ring in *3*. Protein densities surrounding the membrane tube (*1* and *2*) or central lipid dome (*3*) have a width of 5 nm, consistent with the C2AB domain of SYT. (*B*) Diffraction pattern of the tube (shown in *A*) computed by fast Fourier transform. The two principal helices ($n_{1,0}$ = −4, $n_{0,1}$ = 22) are indicated. The arrow points to the last visible layer line at 39 Å. (*C*) Surface representation of the (−4, 22) SYT tube reconstructed from five negatively stained tubes using SPARX-IHRSR. The rise/subunit and the rotation/subunit were calculated from the helical symmetry. The axial dimension of a single of layer of the ring (denoted by the arrow) is 40 Å.

uniform diameter, yielding blurry 2D class averages that failed to resolve the subunit of the ring (Fig. 2*D* and Fig. S6). At the current resolution (24.2 Å) of the EM map, we are unable to distinguish whether the C2A or C2B domain interacts with the membrane, but a reasonable interpretation, given that the site I mutation (K326A, K327A) strongly reduced ring formation (Fig. S2), places the C2B domain on the protein/lipid interface in our EM map (Fig. S7). It should be noted that the elongation of SYT-coated membrane tubes may not occur in a physiological setting because the growth of these SYT arrays will be limited by the amount of SYT present on each synaptic vesicle and by the length of the juxtamembrane linker (~60 residues) that connects the C2 domains to the membrane anchor in the synaptic vesicle. Thus the SYT ring is unlikely to grow more than one layer under in vivo conditions.

Calcium Disrupts the SYT Rings. In our early attempts, we observed that calcium prevented the assembly of SYT rings (Fig. S1). To exclude the possibility that any given divalent cation may interfere with ring formation, we tested if SYT rings can exist in the presence of magnesium (Mg^{2+}) at a physiological level (1 mM Mg^{2+}). Although Mg^{2+} present in the protein incubation buffer did not affect the structural features of SYT rings, it reduced the total number of rings observed (with Mg^{2+} condition: 3.3 ± 0.4 rings per um^2; non-Mg^{2+} condition: 9.9 ± 0.9 rings per um^2; $P < 0.001$) (Fig. S2). This reduction might be caused by the ability of Mg^{2+} to cluster PS and/or shield electrostatic interaction between SYT and the lipid.

Next, we tested if calcium disrupted preformed SYT rings. SYT-C2AB rings formed in the presence of 1 mM Mg^{2+} were rinsed briefly (~10 s) with the same incubation buffer without or with calcium (0.1 mM or 0.5 mM Ca^{2+}) before negative staining. As shown in Fig. 4*A*, even a brief treatment with calcium drastically disrupted the integrity of SYT rings. Inclusion of 0.1 mM Ca^{2+} in the wash buffer resulted in more fragmented and incomplete rings, and the number of SYT rings remaining after the calcium wash decreased proportionally to increasing concentrations of Ca^{2+} present in the wash buffer. In contrast, the number of rings remained approximately constant for the EM grid rinsed with magnesium buffer (with Mg^{2+} rinse: 3.3 ± 0.4 ring per um^2; without Mg^{2+} rinse: 3.8 ± 0.3 ring per um^2; $P > 0.1$), indicating that the disruption of rings is calcium-specific. Although ring-like features disappeared after the Ca^{2+} rinse, SYT remained bound to the lipid surface. The disruption of SYT rings was reversed when Ca^{2+} was chelated with EDTA (Fig. S8).

To verify that the calcium sensitivity of the SYT rings reflects a specific interaction of Ca^{2+} with SYT, we generated an SYT mutant, 3xDA (D309A, D363A, D365A), in which the Ca^{2+} binding to the C2B, the principle domain involved in triggering neurotransmitter release (16), was disrupted. Consistent with earlier observations (12, 38), SYT 3xDA showed impaired ability to cluster liposomes in response to calcium (Fig. S9) but was capable of self-assembling into ring-like structures (Fig. 4*B*). We observed a greater number of rings formed in the 3xDA mutant than in the WT SYT (3xDA: 8.4 ± 0.7 ring per um^2; WT: 3.8 ± 0.3 ring per um^2; $P < 0.001$), probably reflecting enhanced electrostatic interaction between the lipid and SYT in the absence of Ca^{2+} because the cluster of negative-charged aspartic residues was neutralized by the alanine mutations. Nevertheless, the 3xDA rings were insensitive to washing by calcium buffer; in fact, the number of ring-like structures increased after calcium treatment (Fig. 4*B*), probably mediated by the association of the calcium-bound C2A domain with the lipid monolayer. These data clearly show that the Ca^{2+} sensitivity of SYT rings is caused by the calcium-binding site of the C2B domain.

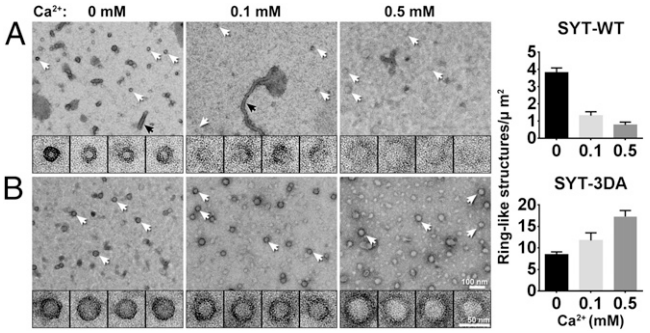

Fig. 4. The SYT-C2AB ring is disrupted by calcium ions. (*A*) Electron micrographs of WT SYT-C2AB rings rinsed briefly with 1 mM Mg^{2+} (*Left*) or with buffer containing 1 mM Mg^{2+} supplemented with 0.1 mM (*Center*) or 0.5 mM (*Right*) Ca^{2+}. The number of ring-like structures is reduced as a function of free calcium concentration. Black arrows indicate tubules. *Insets* show the enlarged rings or fragmented rings indicated by white arrows. (*B*) Electron micrographs of rings of the calcium-binding site mutant SYT-3xDA (SYT D309A, D363A, D365A). The calcium-induced disassembly of the ring is abolished by disrupting the calcium-binding ability of the C2B domain. Quantifications of SYT-C2AB ring-like structures maintained on the lipid monolayer as a function of free calcium for both WT SYT and the calcium-binding mutant SYT-3xDA are shown at the far right. Summary graphs show mean ± SEM ($n = 3$, >40 micrographs per condition).

Discussion

Here we report the unexpected observation that the cytosolic domain of SYT can form ring-like oligomers on lipid surfaces in the absence of calcium. If these rings were to form at the interface of the synaptic vesicles and the plasma membrane, they would act as a "washer" to separate these membranes and thereby sterically prevent the completion of SNARE-dependent fusion (Fig. 5). Then it would be simple to imagine that calcium-triggered disassembly of the ring would allow the resumption and completion of fusion. The height of the ring [about 4 nm as estimated from SYT-tube reconstruction (Fig. 3*C*)] and the distance between membranes bridged by the C2AB domain (39) would allow the N-terminal (membrane-distal) domain of the SNARE complex to assemble, but such a gap would impede the complete assembly of the SNARE complex (40). As a result, the SYT ring would act as a "clamp" on neurotransmitter release.

Why would rings be disassembled by calcium? The simplest explanation, based on the site I (calcium-independent) interaction with acidic membrane lipids, would be that the SYT molecule in the ring assembly orients so that site II is held back from membrane penetration (Fig. S7). The insertion of site II upon calcium binding then would require the reorientation of the ring geometry. Additionally, intramolecular interactions (41) and alternative oligomeric arrangements formed uniquely in the presence of calcium (42) may destabilize further the calcium-free rings we have described here. The calcium-triggered membrane insertion could accelerate fusion further by inducing local curvature to lower the energy for bilayer merging (11, 31, 43). Thus this simple spacer (washer model) (Fig. 5) could explain how SYT acts both as a clamp and an activator of neurotransmitter release, synchronizing the release to Ca^{2+} influx (44, 45).

The clamping role of CPX involves a transacting mechanism that would stabilize the precisely half-zippered SNARE intermediate (24). Deletion of CPX results in a higher rate of spontaneous neurotransmitter release and a reduced amount of evoked release that generally is less synchronous (46–50). Thus, CPX adds a layer of regulation that reduces noise, increases signal, and allows more precise timing for information processing by neural circuitry. It is possible to imagine that the "zig-zag array" of transclamped CPX-SNAREpins (24) is itself templated by the ring by virtue of the binding of constituent t-SNAREs to

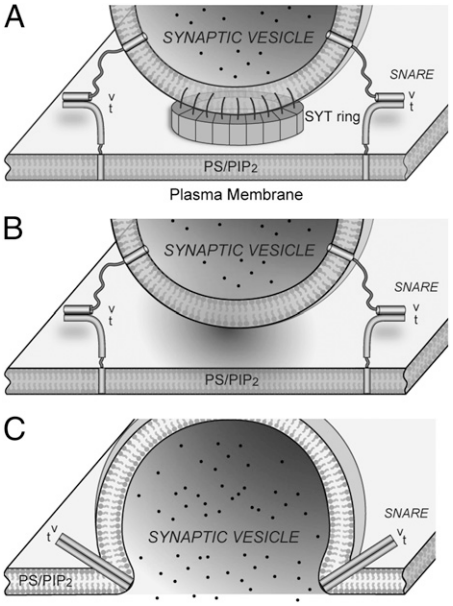

Fig. 5. Schematics of the SYT ring during calcium-triggered neurotransmitter release. (*A*) In the absence of calcium, SYTs emanating from the synaptic vesicle are recruited to the plasma membrane surface by interacting with anionic lipids, such as PS and PIP_2. The locally enriched SYTs form a ring-like oligomer that serves as a physical barrier to separate opposing membrane bilayers and constrain the zippering of SNARE complexes at their N termini. This diagram is drawn to scale with a SYT ring 25 nm in diameter corresponding to 16 copies of SYT in a 50-nm vesicle (32). (*B*) Localized calcium influx causes the reorientation of the SYT molecules on membrane surface, thus disrupting the SYT/SYT interaction necessary for the circular arrangement. As a result, the physical barrier to membrane fusion disappears. (*C*) Partially assembled SNARE complexes resume and complete the zippering that results in membrane fusion and the rapid release of neurotransmitters.

the proposed SYT ring. Obviously, this model is speculative, and further structural and physiological studies will be required to ascertain its relevance.

Consistent with the washer model, it is known that the initial docking of the synaptic vesicles to the plasma membrane is independent of SNARE complex assembly (18, 51, 52) and involves SYT from the synaptic vesicle binding the acidic lipids, including PIP_2 in the plasma membrane (9, 53–56). Furthermore, although deletion of CPX markedly increases the amount of spontaneous transmitter release and reduces the amount of calcium-coupled release, much release still remains (provided SYT remains) (46, 49, 57–59). In further support of this model, it has been shown that SYT by itself can act a negative regulator (clamp) of SNARE-mediated fusion under Ca^{2+}-free conditions (12, 41, 44, 45), and synaptic transmission is inhibited more severely in mutations that abolish the membrane insertion of C2B domain than in SYT-null mutants (14).

The calcium-independent ring assembly is not constrained to a rigid number of subunits. Rings and ring-related tubes of various diameters can be found in our monolayer system (Fig. 2*A* and Fig. S4). Helical indexing of SYT tubes 37 nm in diameter showed 22-fold symmetry (i.e., 22 SYT molecules per ring) (Fig. 3). Therefore, we estimate that rings 18–43 nm in diameter would comprise 11–25 copies of SYT (Fig. 2*A*). There are ∼16–22 copies of SYT on a synaptic vesicle (40–50 nm) (5, 60), enough to form a ring ∼27–37 nm in diameter, assuming that copies originating from the transient plasma membrane pool of SYT do not contribute (Fig. 5). Besides neurotransmitter release, other types of calcium-dependent exocytosis use larger (200–350 nm) vesicles, such as the neuropeptide-containing dense-core vesicles and hormone-containing secretory granules (61, 62), which may harbor more SYT and allow the assembly of larger rings.

The self-organization of SYT into the rings might provide a scaffold for the organization of other components of the membrane fusion machinery under resting conditions to allow rapid and synchronous fusion upon calcium influx. The intrinsic calcium cooperativity of synaptic exocytosis suggests that multiple Ca^{2+} ions are required to activate SYT (63). It is estimated that 3–5 Ca^{2+} ions are required to trigger synchronized exocytosis (64, 65), but reduced calcium-binding affinity does not change the calcium cooperativity of neurotransmitter release (66), suggesting that multiple copies of SYT might be involved in gating release. This notion is consistent with our current model in which the oligomeric nature of the SYT ring allows a few calcium ions stochastically binding to several subunits within the ring to result in the rapid disintegration of the SYT ring and thus triggering fusion.

Materials and Methods

Details of materials and methods are provided in *SI Materials and Methods*. GST-SYT-C2AB was expressed in *Escherichia coli* BL21(DE3) and was purified as previously described (10). EM on lipid monolayers was carried out as described (29). Briefly, lipid monolayers formed at the air/water interface were recovered by a carbon-coated EM grid (400 mesh; Ted Pella). Then protein solution was added to the lipid side of the grid and was incubated in a humidity chamber. After brief rinsing with incubation buffer supplemented with $Mg(AC)_2$ or $CaCl_2$ at various concentrations, the grid was blotted, negatively stained with uranyl acetate solution (1% wt/vol), and air dried. To prepare a sample for cryo-EM, the monolayer was picked up with a Quantifoil 2/2 grid (SPI Supplies) with the carbon side facing the lipid. The grid was incubated with SYT-C2AB and plunge-frozen into liquid ethane using a Vitrobot (FEI). The samples were examined on a Tecnai T12 microscope (FEI) operated at an acceleration voltage of 120 kV. Images were recorded under low-dose conditions (∼20 $e^-/Å^2$) on a 4K × 4K CCD camera (Gatan), at a nominal magnification of 42,000×. For image processing, SYT-C2AB ring complexes were aligned to a set of disk references 15–45 nm in diameter using multireference alignment in Imagic (67). SYT-C2AB–decorated tubes were indexed further with the EMIP program suite (68) to determine the helical symmetry. Tubes having the same diameter, as determined by projection matching, and indexed as being in the same helical family were combined and subjected to IHRSR using sxihrsr (37). The crystal structure of SYT-C2AB [Protein Data Bank (PDB) ID code 2R83] was placed manually into the EM maps of the SYT-decorated tube and then was fitted using the fit-in-map function of Chimera (69).

ACKNOWLEDGMENTS. We thank Dr. Daniel Lévy and Dr. Liguo Wang for advice on setting up the lipid monolayer assay. This work was supported by grant from the National Institutes of Health Grant GM 071458 (to J.E.R.).

1. Brose N, Petrenko AG, Südhof TC, Jahn R (1992) Synaptotagmin: A calcium sensor on the synaptic vesicle surface. *Science* 256(5059):1021–1025.
2. Geppert M, et al. (1994) Synaptotagmin I: A major Ca2+ sensor for transmitter release at a central synapse. *Cell* 79(4):717–727.
3. Fernández-Chacón R, et al. (2001) Synaptotagmin I functions as a calcium regulator of release probability. *Nature* 410(6824):41–49.
4. Chapman ER (2008) How does synaptotagmin trigger neurotransmitter release? *Annu Rev Biochem* 77:615–641.
5. Takamori S, et al. (2006) Molecular anatomy of a trafficking organelle. *Cell* 127(4):831–846.
6. Li C, et al. (1995) Ca(2+)-dependent and -independent activities of neural and non-neural synaptotagmins. *Nature* 375(6532):594–599.
7. Bai J, Tucker WC, Chapman ER (2004) PIP2 increases the speed of response of synaptotagmin and steers its membrane-penetration activity toward the plasma membrane. *Nat Struct Mol Biol* 11(1):36–44.
8. Kuo W, Herrick DZ, Ellena JF, Cafiso DS (2009) The calcium-dependent and calcium-independent membrane binding of synaptotagmin 1: Two modes of C2B binding. *J Mol Biol* 387(2):284–294.
9. Parisotto D, Malsam J, Scheutzow A, Krause JM, Söllner TH (2012) SNAREpin assembly by Munc18-1 requires previous vesicle docking by synaptotagmin 1. *J Biol Chem* 287(37):31041–31049.
10. Seven AB, Brewer KD, Shi L, Jiang QX, Rizo J (2013) Prevalent mechanism of membrane bridging by synaptotagmin-1. *Proc Natl Acad Sci USA* 110(34):E3243–E3252.

11. Martens S, Kozlov MM, McMahon HT (2007) How synaptotagmin promotes membrane fusion. *Science* 316(5828):1205–1208.
12. van den Bogaart G, et al. (2011) Synaptotagmin-1 may be a distance regulator acting upstream of SNARE nucleation. *Nat Struct Mol Biol* 18(7):805–812.
13. Paddock BE, Striegel AR, Hui E, Chapman ER, Reist NE (2008) Ca2+-dependent, phospholipid-binding residues of synaptotagmin are critical for excitation-secretion coupling in vivo. *J Neurosci* 28(30):7458–7466.
14. Paddock BE, et al. (2011) Membrane penetration by synaptotagmin is required for coupling calcium binding to vesicle fusion in vivo. *J Neurosci* 31(6):2248–2257.
15. Rhee JS, et al. (2005) Augmenting neurotransmitter release by enhancing the apparent Ca2+ affinity of synaptotagmin 1. *Proc Natl Acad Sci USA* 102(51):18664–18669.
16. Mackler JM, Drummond JA, Loewen CA, Robinson IM, Reist NE (2002) The C(2)B Ca(2+)-binding motif of synaptotagmin is required for synaptic transmission in vivo. *Nature* 418(6895):340–344.
17. Rickman C, Davletov B (2003) Mechanism of calcium-independent synaptotagmin binding to target SNAREs. *J Biol Chem* 278(8):5501–5504.
18. de Wit H, et al. (2009) Synaptotagmin-1 docks secretory vesicles to syntaxin-1/SNAP-25 acceptor complexes. *Cell* 138(5):935–946.
19. Choi UB, et al. (2010) Single-molecule FRET-derived model of the synaptotagmin 1-SNARE fusion complex. *Nat Struct Mol Biol* 17(3):318–324.
20. Krishnakumar SS, et al. (2013) Conformational dynamics of calcium-triggered activation of fusion by synaptotagmin. *Biophys J* 105(11):2507–2516.
21. Mohrmann R, et al. (2013) Synaptotagmin interaction with SNAP-25 governs vesicle docking, priming, and fusion triggering. *J Neurosci* 33(36):14417–14430.
22. Pang ZP, Shin OH, Meyer AC, Rosenmund C, Südhof TC (2006) A gain-of-function mutation in synaptotagmin-1 reveals a critical role of Ca2+-dependent soluble N-ethylmaleimide-sensitive factor attachment protein receptor complex binding in synaptic exocytosis. *J Neurosci* 26(48):12556–12565.
23. Giraudo CG, Eng WS, Melia TJ, Rothman JE (2006) A clamping mechanism involved in SNARE-dependent exocytosis. *Science* 313(5787):676–680.
24. Kümmel D, et al. (2011) Complexin cross-links prefusion SNAREs into a zigzag array. *Nat Struct Mol Biol* 18(8):927–933.
25. Tang J, et al. (2006) A complexin/synaptotagmin 1 switch controls fast synaptic vesicle exocytosis. *Cell* 126(6):1175–1187.
26. Malsam J, et al. (2012) Complexin arrests a pool of docked vesicles for fast Ca(2+)-dependent release. *EMBO J* 31(15):3270–81.
27. Krishnakumar SS, et al. (2011) A conformational switch in complexin is required for synaptotagmin to trigger synaptic fusion. *Nat Struct Mol Biol* 18(8):934–940.
28. Solodukhin AS, Caldwell HL, Sando JJ, Kretsinger RH (2002) Two-dimensional crystal structures of protein kinase C-delta, its regulatory domain, and the enzyme complexed with myelin basic protein. *Biophys J* 82(5):2700–2708.
29. Kelly DF, Abeyrathne PD, Dukovski D, Walz T (2008) The Affinity Grid: A pre-fabricated EM grid for monolayer purification. *J Mol Biol* 382(2):423–433.
30. Fuson KL, Montes M, Robert JJ, Sutton RB (2007) Structure of human synaptotagmin 1 C2AB in the absence of Ca2+ reveals a novel domain association. *Biochemistry* 46(45): 13041–13048.
31. Hui E, Johnson CP, Yao J, Dunning FM, Chapman ER (2009) Synaptotagmin-mediated bending of the target membrane is a critical step in Ca(2+)-regulated fusion. *Cell* 138(4):709–721.
32. Fukuda M, Kanno E, Ogata Y, Mikoshiba K (2001) Mechanism of the SDS-resistant synaptotagmin clustering mediated by the cysteine cluster at the interface between the transmembrane and spacer domains. *J Biol Chem* 276(43):40319–40325.
33. Lu B, Kiessling V, Tamm LK, Cafiso DS (2014) The Juxta-Membrane Linker of Full-Length Synaptotagmin 1 Controls Oligomerization and Calcium-Dependent Membrane Binding. *J Biol Chem* 289(32):22161–71.
34. Baoukina S, Monticelli L, Risselada HJ, Marrink SJ, Tieleman DP (2008) The molecular mechanism of lipid monolayer collapse. *Proc Natl Acad Sci USA* 105(31):10803–10808.
35. Toyoshima C (2000) Structure determination of tubular crystals of membrane proteins. I. Indexing of diffraction patterns. *Ultramicroscopy* 84(1-2):1–14.
36. Egelman EH (2007) The iterative helical real space reconstruction method: Surmounting the problems posed by real polymers. *J Struct Biol* 157(1):83–94.
37. Behrmann E, et al. (2012) Real-space processing of helical filaments in SPARX. *J Struct Biol* 177(2):302–313.
38. Hui E, et al. (2011) Mechanism and function of synaptotagmin-mediated membrane apposition. *Nat Struct Mol Biol* 18(7):813–821.
39. Araç D, et al. (2006) Close membrane-membrane proximity induced by Ca(2+)-dependent multivalent binding of synaptotagmin-1 to phospholipids. *Nat Struct Mol Biol* 13(3):209–217.
40. Li F, et al. (2007) Energetics and dynamics of SNAREpin folding across lipid bilayers. *Nat Struct Mol Biol* 14(10):890–896.
41. Liu H, et al. (2014) Linker mutations reveal the complexity of synaptotagmin 1 action during synaptic transmission. *Nat Neurosci* 17(5):670–677.
42. Wu Y, et al. (2003) Visualization of synaptotagmin I oligomers assembled onto lipid monolayers. *Proc Natl Acad Sci USA* 100(4):2082–2087.
43. Chernomordik LV, Kozlov MM (2003) Protein-lipid interplay in fusion and fission of biological membranes. *Annu Rev Biochem* 72:175–207.
44. Littleton JT, Stern M, Perin M, Bellen HJ (1994) Calcium dependence of neurotransmitter release and rate of spontaneous vesicle fusions are altered in Drosophila synaptotagmin mutants. *Proc Natl Acad Sci USA* 91(23):10888–10892.
45. Chicka MC, Hui E, Liu H, Chapman ER (2008) Synaptotagmin arrests the SNARE complex before triggering fast, efficient membrane fusion in response to Ca2+. *Nat Struct Mol Biol* 15(8):827–835.
46. Jorquera RA, Huntwork-Rodriguez S, Akbergenova Y, Cho RW, Littleton JT (2012) Complexin controls spontaneous and evoked neurotransmitter release by regulating the timing and properties of synaptotagmin activity. *J Neurosci* 32(50):18234–18245.
47. Cao P, Yang X, Südhof TC (2013) Complexin activates exocytosis of distinct secretory vesicles controlled by different synaptotagmins. *J Neurosci* 33(4):1714–1727.
48. Hobson RJ, Liu Q, Watanabe S, Jorgensen EM (2011) Complexin maintains vesicles in the primed state in C. elegans. *Curr Biol* 21(2):106–113.
49. Huntwork S, Littleton JT (2007) A complexin fusion clamp regulates spontaneous neurotransmitter release and synaptic growth. *Nat Neurosci* 10(10):1235–1237.
50. Reim K, et al. (2001) Complexins regulate a late step in Ca2+-dependent neurotransmitter release. *Cell* 104(1):71–81.
51. Geumann U, Barysch SV, Hoopmann P, Jahn R, Rizzoli SO (2008) SNARE function is not involved in early endosome docking. *Mol Biol Cell* 19(12):5327–5337.
52. Toonen RF, et al. (2006) Dissecting docking and tethering of secretory vesicles at the target membrane. *EMBO J* 25(16):3725–3737.
53. Honigmann A, et al. (2013) Phosphatidylinositol 4,5-bisphosphate clusters act as molecular beacons for vesicle recruitment. *Nat Struct Mol Biol* 20(6):679–686.
54. Kim JY, et al. (2012) Solution single-vesicle assay reveals PIP2-mediated sequential actions of synaptotagmin-1 on SNAREs. *EMBO J* 31(9):2144–2155.
55. Reist NE, et al. (1998) Morphologically docked synaptic vesicles are reduced in synaptotagmin mutants of Drosophila. *J Neurosci* 18(19):7662–7673.
56. Wang Z, Liu H, Gu Y, Chapman ER (2011) Reconstituted synaptotagmin I mediates vesicle docking, priming, and fusion. *J Cell Biol* 195(7):1159–1170.
57. Cho RW, Song Y, Littleton JT (2010) Comparative analysis of Drosophila and mammalian complexins as fusion clamps and facilitators of neurotransmitter release. *Mol Cell Neurosci* 45(4):389–397.
58. Xue M, et al. (2009) Tilting the balance between facilitatory and inhibitory functions of mammalian and Drosophila Complexins orchestrates synaptic vesicle exocytosis. *Neuron* 64(3):367–380.
59. Martin JA, Hu Z, Fenz KM, Fernandez J, Dittman JS (2011) Complexin has opposite effects on two modes of synaptic vesicle fusion. *Curr Biol* 21(2):97–105.
60. Wilhelm BG, et al. (2014) Composition of isolated synaptic boutons reveals the amounts of vesicle trafficking proteins. *Science* 344(6187):1023–1028.
61. Wang CT, et al. (2001) Synaptotagmin modulation of fusion pore kinetics in regulated exocytosis of dense-core vesicles. *Science* 294(5544):1111–1115.
62. Gerber SH, Südhof TC (2002) Molecular determinants of regulated exocytosis. *Diabetes* 51(Suppl 1):S3–S11.
63. Matveev V, Bertram R, Sherman A (2011) Calcium cooperativity of exocytosis as a measure of Ca^2+ channel domain overlap. *Brain Res* 1398:126–138.
64. Schneggenburger R, Neher E (2000) Intracellular calcium dependence of transmitter release rates at a fast central synapse. *Nature* 406(6798):889–893.
65. Schneggenburger R, Neher E (2005) Presynaptic calcium and control of vesicle fusion. *Curr Opin Neurobiol* 15(3):266–274.
66. Striegel AR, et al. (2012) Calcium binding by synaptotagmin's C2A domain is an essential element of the electrostatic switch that triggers synchronous synaptic transmission. *J Neurosci* 32(4):1253–1260.
67. van Heel M, Harauz G, Orlova EV, Schmidt R, Schatz M (1996) A new generation of the IMAGIC image processing system. *J Struct Biol* 116(1):17–24.
68. Diaz R, Rice WJ, Stokes DL (2010) Fourier-Bessel reconstruction of helical assemblies. *Methods Enzymol* 482:131–165.
69. Goddard TD, Huang CC, Ferrin TE (2007) Visualizing density maps with UCSF Chimera. *J Struct Biol* 157(1):281–287.